IEEE Access
Multidisciplinary | Rapid Review | Open Access Journal

Received January 17, 2022, accepted February 7, 2022, date of publication February 9, 2022, date of current version February 17, 2022.

Digital Object Identifier 10.1109/ACCESS.2022.3150344

Day-Ahead Short-Term Load Forecasting for Holidays Based on Modification of Similar Days' Load Profiles

JIHOO SON[1], JIWON CHA[1], (Graduate Student Member, IEEE), HYUNSU KIM[2], AND YOUNG-MIN WI[3]

[1]School of Electrical Engineering, Korea University, Seoul 02841, Republic of Korea
[2]Korea Power Exchange, Naju 58322, Republic of Korea
[3]School of Electrical and Electronic Engineering, Gwangju University, Gwangju 61743, Republic of Korea

Corresponding author: Young-Min Wi (ymwi@gwangju.ac.kr)

This work was supported in part by the National Research Foundation of Korea (NRF) Grant funded by the Korea Government [Ministry of Science and ICT (MSIT)] under Grant 2020R1C1C1013228 and Grant 2020R1A4A1019405; and in part by the Research Funds from Gwangju University, in 2022.

ABSTRACT Short-term load forecasting (STLF) is necessary for system operators; however, its difficulty has been increasing since distributed resources, particularly behind-the-meter (BTM) PV resources, have been introduced to power systems. This study proposes a framework for STLF for holidays considering the four major factors that affect the net load profiles —calendar, trend, weather, and BTM PV. The target holiday is first paired with historical holidays following its calendar factor, which are defined as ''similar days.'' Subsequently, in terms of the remaining three factors, the differences between the historical holidays and target holidays are calculated, and their effects on load differences (factor-induced load differences) are quantified and reflected. Finally, for each pair, the modified load profiles are generated and combined to obtain a daily load profile of the target holiday. The proposed framework was implemented on a case study of Korean national holidays, and its forecasting accuracy was compared with conventional forecasting methods. The accuracy metrics show that the proposed framework outperforms conventional methods. The results suggest that the proposed framework can be applied to STLF for holidays to improve forecasting accuracy.

INDEX TERMS BTM PV resources, genetic algorithm, holiday load forecasting, short-term load forecasting, weather sensitivity.

I. INTRODUCTION

Day-ahead short-term load forecasting (STLF) is implemented daily to ensure the reliability of a power system and to establish a power-generation schedule. Through accurate forecasting, power systems can be operated cost-effectively, and decisions regarding unit commitment and energy markets can be made correctly.

The daily load profile is closely associated with numerous factors that have different impacts on the load profile, such as economic growth, human activity, and weather conditions. The main challenge associated with STLF is that these factors overlap and affect load profiles simultaneously. In addition, their impacts on load are dynamic rather than static. Thus, each ''factor-induced load'' must be disintegrated from the historical load profiles and quantified for accurate forecasting. Load profiles are affected by the ''calendar effect'' and ''weather effect.'' They have a major impact on the intraday pattern and the level of load profiles. Additionally, over a long term, the base load changes because economic growth affects the total electricity consumption. Recently, the most critical issue in the power system has been the increasing penetration of distributed resources that are known to be particularly variable and uncertain. This issue could be a barrier to system security and optimal operation [1]. Owing to the high variance of distributed resources' generation output, considering the generation of distributed resources when operating power systems and markets has become significant [2]. Among the distributed resources, behind-the-meter (BTM) resources are unobservable and therefore pose a major challenge in the field of load forecasting. BTM resources, especially BTM photovoltaics (PV), significantly

The associate editor coordinating the review of this manuscript and approving it for publication was Shiwei Xia.

reduce the net load profiles. Therefore, it is necessary to consider BTM PV generation when performing STLF. Research on PV generation forecasting has increased rapidly over the past few years. In addition, several attempts have been made to associate solar power forecasting with load forecasting [3]. A wide variety of load forecasting methodologies have been developed in previous research. A univariate STLF model has been proposed [4] based on the linear regression and historical pattern of load, where the training set for fitting a regression model is composed of the k-nearest neighbors of an input load profile. A seasonal autoregressive integrated moving average with exogenous variables (sarimax) model, which is a type of time series model, has also been proposed [5]. The regarded external variables include lagged hourly load data and calendar effects. Despite their high explanatory power, models based on regression or time series models require a much higher level of sophisticated work in modeling the relationship between explanatory variables and response variables, such as selecting features and capturing weather effects.

Moreover, a machine learning-based method has been attracting attention due to its high prediction accuracy. A deep neural network algorithm utilizing historical load patterns as input variables has been proposed [6]. The model in [6] uses a convolutional neural network (CNN) for feature extraction from historical load data. In [7], an artificial neural network (ANN) for STLF has been proposed, which considers various combinations of load data as input variables. In [8], a bat algorithm-based backpropagation approach is introduced, which utilizes weather factors such as temperature and humidity and reduces the requirements of trial and error in a training phase. In [9], Long Short-Term memory (LSTM) and an ensemble algorithm XGBoost shows better accuracy than ARIMA in predicting time series data. XGBoost has also been adopted as a short-term load forecasting method in [10]. However, the use of forecasting models based on machine learning has limitations: the models require high computing capability and sufficient data for the training phase, and it is difficult to interpret their output and weights.

In the case of holidays, load forecasting is challenging because of the following reasons: (1) The calendar effect is dominant on holidays; thus, the load profiles of holidays show unique patterns and have been treated as anomalous observations. (2) Holidays occur infrequently, even irregularly, so the historical data are insufficient. (3) Since various factors as well as calendar factors influence load profiles of holidays in different ways, it is difficult to quantify the impact of individual factors. Previous studies have proposed holiday load forecasting methods using load profiles of past holidays based on the assumption that the future shares a similar pattern and distribution as the historical data [1]. These studies have primarily employed statistical-based methods since the machine-learning-based forecasting model requires a sufficient amount of training data to build an accurate forecasting engine; however, historical data on holidays are insufficient. In [11], a regression-based holiday load forecasting model has been designed for the public holidays of Germany, and several approaches to deal with holidays are analyzed. In [12], a rule-based autoregressive moving average model for French public holidays has been proposed. The model proposed in [12] considers intraday, intraweek, and intrayear seasonality using a SARMA model. However, external effects such as the weather effect have not been considered in [11] and [12]. In [13], a classification for special days has been presented, and a linear regression has been adopted to model the effect of holidays on the load considering categorical variables that identify each type of holiday. However, only the temperature-derived weather features, such as cooling and heating degree days, have been considered as exogenous variables. A hybrid prediction model for holiday load forecasting has also been proposed. In [14], holiday load profiles are decomposed into daily extremum and load shape and both are predicted independently using the load profiles of similar days. The daily extremum of load profiles is predicted by a machine learning model (XGBoost), and the hourly load shape is obtained from the mean of similar dates' historical load shapes. In [15], a fuzzy linear regression model is employed for short-term load forecasting on holidays and is built from the load data of previous years. Moreover, a fuzzy polynomial regression method for holidays and a process of weather feature selection using mutual information have been proposed [16]. However, these models do not consider BTM PV generation and adopt a simple mean for forecasting the normalized hourly pattern of load profiles on holidays.

The differences between the models proposed in the literature are tabulated in Table 1. The related studies are compared in terms of forecasting target, methodology, and input data. Among the previous approaches, only a few studies have attempted to consider various weather features as input variables and the BTM PV effect in the prediction of holidays' load profiles. Moreover, several methods that utilize historical load have adopted a simple mean approach for forecasting the hourly load shape of target holidays. Due to the aforementioned problems, this study proposes a framework for holiday load forecasting that considers four major factors: calendar, trend, weather, and BTM PV. Given a target holiday, pairs of similar days are selected, and each load profile of a similar day is modified by quantifying the load differences (factor-induced load) in terms of each factor. The modified load profiles of similar days are combined to provide a final load forecasting for the target holiday. The main contributions of this study are as follows.

1) To reflect the calendar effect on each target holiday, an in-depth analysis of historical load profiles of Korean holidays is presented, and a rule-based similar day selection process is proposed. Korean holidays are classified into two types according to their historical load profiles, and a set of similar days are determined according to the given target holiday's holiday type and day of the week.

TABLE 1. Detail comparison of related works.

Forecasting target	No.	Methodology	Brief descriptions for input data considered in the literature
Normal days	[4]	Regression	Historical load
	[5]	SARIMAX	Historical load Calendar
	[6]	Neural network	Historical load
	[7]	Neural network	Historical load
	[8]	Neural network	Historical load Weather (temperature and humidity)
	[10]	Ensemble learning	Historical load
Holidays	[11]	Regression	Historical load Calendar
	[12]	SARMA	Historical load Calendar
	[13]	Regression	Historical load Weather (temperature, heating degree days, and cooling degree days) Calendar
	[14]	Ensemble learning	Historical load Weather (temperature) Calendar data
	[15]	Regression	Historical load
	[16]	Regression	Historical load Weather (daily minimum/peak/average temperature, duration of sunshine, relative humidity, wind speed, and discomfort index)

2) Various weather features related to load profiles are introduced, and adaptive weather feature selection is implemented to determine a set of input weather features. A total of 20 weather features are classified into ''primary features'' or ''secondary features,'' depending on how each feature is created. Weather features are evaluated based on the statistical analysis of historical weather observations and forecasts. Then, the main idea of ''correlation-based weather feature selection'' is employed to select features relevant to the target variable and not redundant with other weather features.
3) Nonlinearity and time-variant properties of the weather effect are controlled by applying ''weather threshold and sensitivity matrix (WTSM),'' which is defined for every pair of targets and similar days. Regarding the availability of weather forecast data, a ''reference period (RP)'' is introduced to determine the WTSM.
4) A method for combining each modified load profile using adaptive weighted average and determining each weight is proposed, while most published articles adopted a simple mean for the combination.

The remainder of this paper is organized as follows: Section II describes the problem addressed in this paper. Section III proposes the framework and provides a detailed description of the methodology. Section IV describes the performance of the proposed method and discusses the results. Then, the forecasting accuracy of the proposed method is compared with that of the conventional method (fuzzy linear regression). Section V presents a case study on Korean national holidays, conducted to verify the effectiveness of the proposed method.

II. PROBLEM DISCUSSION

For a pair of target holidays and similar days, a load difference between them may exist. The difference is attributed to various factors; therefore, it is necessary to quantify each factor-induced-load difference. Let $LD_{simday}(h)$ and $LD_{target}(h)$ be the historical net load of one similar day at hour h and a net load of the target holiday at hour h, respectively. Thus, a mathematical approximation expressed in (1) can be obtained.

$$LD_{target}(h) \approx \alpha_h \times LD_{simday}(h) + \beta_h, \tag{1}$$

where α_h and β_h represent the coefficients reflecting the load difference between similar days and target holidays. In this study, it is assumed that BTM PV generation forecasts and estimated observations are available for the system operator.

This study aims to design a mathematical model that adjusts the load profiles of similar days to that of the target holiday. It is implemented by incorporating each factor-induced effect on the load. Specifically, a rule-based similar-day selection module is constructed to reflect the calendar effect. It selects historical days according to the target holiday type and the day of the week. In addition, the reconstituted load method is utilized to compensate for the BTM PV effect. Given the observed and forecasted values of BTM PV generation, it compensates for the reduction in the load profile caused by PV generation. The effect of the BTM PV can be eliminated by applying the reconstituted load method. In this method, the historical net load ($NetLD(h)$) is reconstituted by adding the given historical BTM PV generation ($GEN_{BTM}(h)$) into the historical load as follows.

$$RLD(h) = NetLD(h) + GEN_{BTM}(h) \tag{2}$$

TABLE 2. Classification of solar PV resources.

Resources	Metering real-time generation	Tracking capacity
(a)	○	○
(b)		○
(c)		

To forecast the net load ($NetFcstLD(h)$), the system operator subtracts the forecasted BTM generation ($FcstGEN_{BTM}(h)$) from the forecasted reconstituted load ($FcstRLD(h)$) as follows.

$$NetFcstLD(h) = FcstRLD(h) - FcstGEN_{BTM}(h) \quad (3)$$

Then, the trend and weather effects are isolated. The trend effect is incorporated into (1). There are two key steps when estimating the weather effect. First, weather feature selection is performed to adaptively determine a set of input weather features. Second, the WTSM is introduced to reflect the weather sensitivity to the load and is determined by a genetic algorithm (GA).

III. METHODOLOGY

The overall framework of the proposed STLF model is illustrated in Fig. 1. The model consists of three modules: a rule-based similar day selection module, a weather feature selection module, and a load forecasting module where similar days' load profiles are modified using the weather threshold and sensitivity matrix.

A. DATA SET

1) LOAD PROFILE AND PV GENERATION DATA

In this study, two datasets were established: observed data and forecasted data. The former includes historical load profiles, BTM PV generation, and weather observations. The latter includes forecasted weather data and PV generation data. Historical domestic load profile and PV data were acquired from the Korea Power Exchange (KPX) with a 1-h temporal resolution. The PV generation output is the aggregated amount of generation from PV resources. PV resources in Korea are mainly classified into three types according to their trading mechanism, (a) participation in the wholesale electric market, (b) power purchase agreement, and (c) net metering, as shown in Table 2.

BTM PV resources refer to PV resources, and the hourly generation of these resources is invisible to the system operator [17]. Resource (a) participates in the wholesale electric market; thus, such resources are observable to the system operator. In this case, (b) and (c) are BTM PV resources. As the penetration of BTM PV resources increases, they cause a significant decline in the net load and complicate the forecasting of load demand. In practice, the load reconstituting method is applied by independent system operators (ISOs) for load forecasting [18].

TABLE 3. Weather feature comparison dataset.

Weather feature	Unit	Abbrev.	Ref.
Dry-bulb temperature	°C	TA	[19][20]
Relative humidity	%	HM	[19][20]
6-h cumulative precipitation	*mm*	RN	[19][20]
Wind speed	*km/h*	WS	[19][20]
Total cloud cover	-	CC	[19][20]
Solar irradiance	mJ/m^2	SI	-
Cooling degree hours	°C	CDH	[21]
Extra cooling requirements	°C	XCR	-
Heating degree hours	°C	HDH	[21]
Extra heating requirement	°C	XHR	[22]
6-h average temperature	°C	TA06	-
12-h average temperature	°C	TA12	-
24-h average temperature	°C	TA24	-
48-h average temperature	°C	TA48	-
Wet-bulb temperature	°C	TW	[23]
Dew-point temperature	°C	TD	[24]
Wet-bulb Globe Temperature	°C	WBGT	[25]
Discomfort index	%	DI	[26]
Heat index	°C	HI	[27]
Windchill	°C	WC	[28]

2) WEATHER DATA

Weather observation and forecast data from the Korean Meteorological Administration (KMA) were obtained from eight cities (Seoul, Suwon, Incheon, Wonju, Gwangju, Daejeon, Daegu, and Busan). Weather observation data were acquired from the KMA Automated Synoptic Observing System (KMA-ASOS), and weather forecast data were obtained from KMA Local Weather Forecasts (KMA-LWF) and Medium-Range Weather Forecasts (KMA-MRWF).

KMA-LWF publishes weather forecasts eight times a day every three hours. These 3-h interval data were transformed into hourly data by linear interpolation to utilize weather data for hourly load forecasting. Weather forecast data were established considering the availability of data at the forecasting time. Therefore, the forecasting data published at 8:00 a.m. on the forecasting day were used in this study. The weather dataset comprises a total of 20 weather features, including primary and secondary weather features, as shown in Table 3. The primary features refer to raw weather data provided by the weather forecasting system, and the secondary features refer to the features created via feature engineering using primary features. In this study, six primary features (TA, HM, RN, WS, CC, and SI) and 14 secondary features were adopted. Secondary weather features include eight temperature-derived indices (TDIs): CDH, XCR, HDH, XHR, TA06, TA12, TA24, and TA48; five temperature-humidity–derived indices (THIs): TW, TD, HI, WBGT, and DI; and one temperature-wind-speed–derived index (TWI): WC. TDIs are derived by transforming TA, and THIs and TWIs are created by combining primary features. These features are introduced to reflect the compositive and interactive weather effects beyond a single primary weather feature [29].

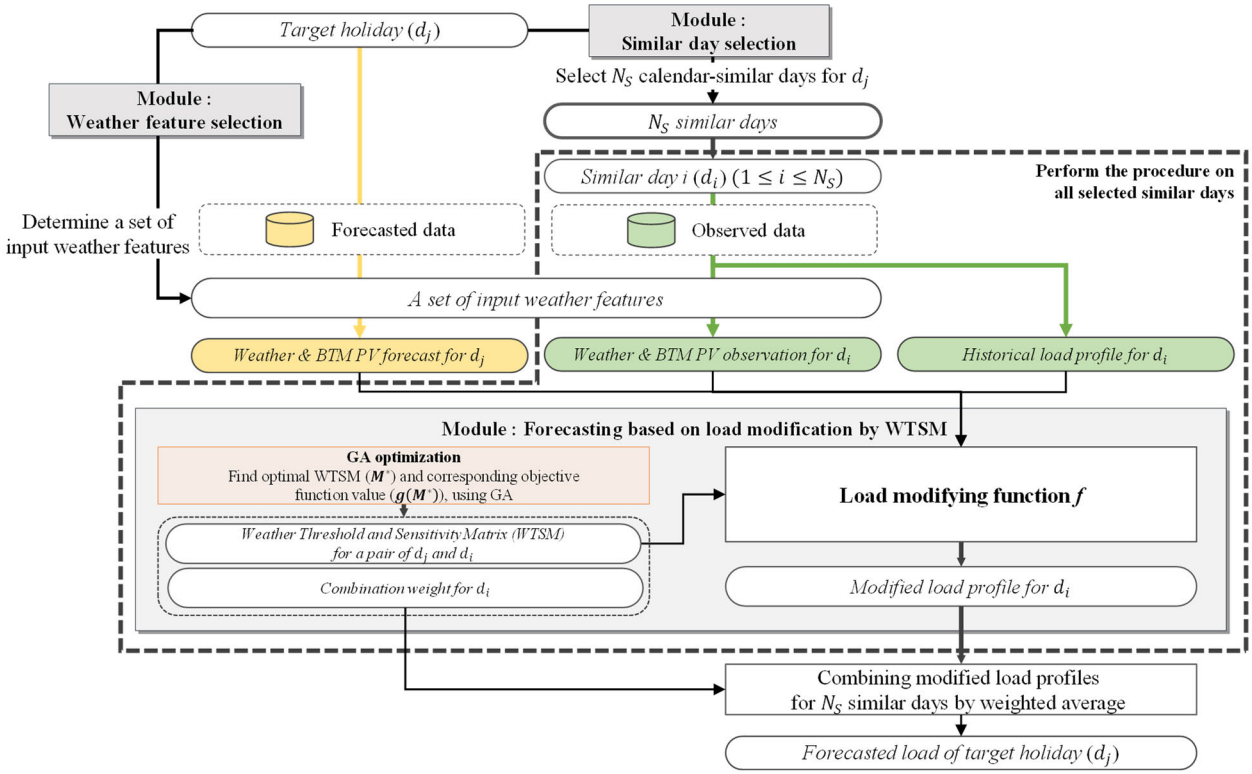

FIGURE 1. The overall framework of the proposed short-term load forecasting method.

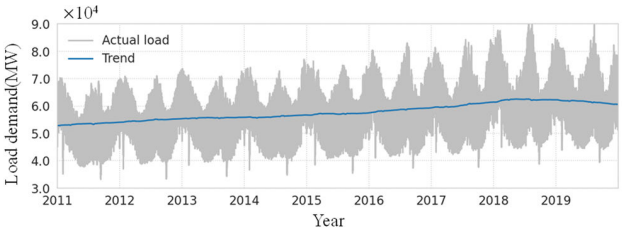

FIGURE 2. Result of time series decomposition of the hourly load demand over 10 years by the period of 8760 h.

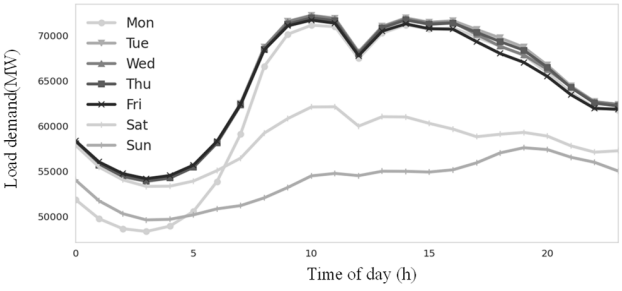

FIGURE 3. Average load profile by DOW for normal days from 2017 to 2018.

B. SELECTING SIMILAR DAYS FOR HOLIDAYS

1) CHARACTERISTICS OF THE HOLIDAY LOAD PROFILE

Compared with normal days, holidays exhibit significant reductions in electric energy consumption and abnormal hourly load patterns. In this study, four attributes (calendar, trend, weather, and BTM PV) were assumed to be the major factors affecting load demand on public holidays. Each of them affects the load profile at different time resolutions, such as yearly, daily, and hourly frames. The trend effect is observed by time series decomposition, as shown in Fig. 2. The overall load consumption has such a trend every year. The calendar attributes create an intraweek cyclic pattern and level along with the day of the week (DOW). Fig. 3 displays the average load profile according to DOW of two years (2017 and 2018). From Tuesday to Friday, the load profiles follow similar patterns. Although Monday is also a weekday, the load profiles in the morning hours are low. Saturdays and Sundays are distinguished from each other by daytime load profiles. Based on the shape of their intraday patterns, they can be classified into four DOW groups as follows:

$$\begin{aligned} \mathrm{DOW}_1 &= \{\mathrm{Mon}\} \\ \mathrm{DOW}_2 &= \{\mathrm{Tue, Wed, Thu, Fri}\} \\ \mathrm{DOW}_3 &= \{\mathrm{Sat}\} \\ \mathrm{DOW}_4 &= \{\mathrm{Sun}\} \end{aligned}$$

In Korea, there are 13 public holidays, most of which follow the Gregorian (solar) calendar, which has fixed dates. However, some Asian cultural countries have holidays that follow the lunar calendar [30]. In Korea, Lunar New Year, Korean Thanksgiving, and Buddha's Birthday follow the lunar calendar. Depending on the year, the Gregorian dates for holidays following the lunar calendar span almost a

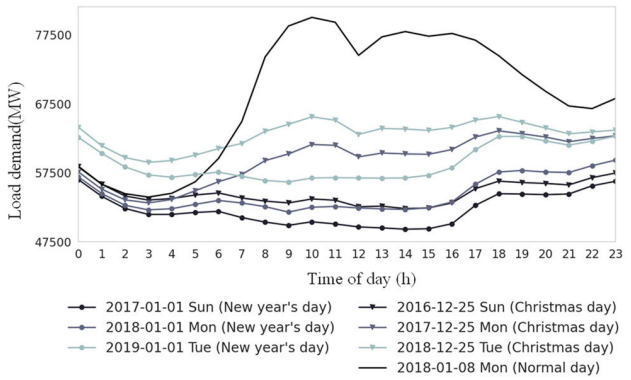

FIGURE 4. Electricity demand on mondays for three weeks, compared with those on corresponding holidays (New year's day and christmas day).

month. Therefore, it is important to separately correct the load demand difference due to the weather difference when performing STLF utilizing the historical load profiles of corresponding holidays. Table 4 describes 13 holidays in Korea, following the lunar calendar (L) or solar calendar (S), and the ranges of their Gregorian dates. Lunar New Year (*Seollal*) and Korean Thanksgiving (*Chuseok*) include three consecutive holidays; thus, each of them is distinguished by a number that follows their abbreviated labels. On holidays, an abnormal electric load pattern and level arise. In Fig. 4, the electric load profiles on Monday for three weeks (December 25, 2017, January 1, 2018, January 8, 2018, which are Christmas Day, New Year's Day, and normal Monday, respectively). Although they are all Mondays, they show different patterns and levels. The load profiles of New Year's Day and Christmas Day demonstrated much lower consumption than that of the following normal day on the same DOW. Given each line plot with dot-shaped markers, which refer to New Year's Days, the daily load profiles of New Year's Days do not follow the typical pattern according to their DOWs, and they exhibit a unique pattern regardless of them. Conversely, by observing the load profiles represented as line plots with triangular-shaped markers, it can be observed that Christmas Days' load profiles exhibit a different pattern based on their DOWs. The load profile of Christmas Day on Sunday (December 25, 2016) showed a drastic decrease of levels during the day compared with those of a Monday (December 25, 2017) and a Tuesday (December 25, 2018). It can be inferred that the hourly load pattern of a holiday follows either a typical pattern of its DOW or a unique pattern of its holiday type.

For a comparison of the shapes of holidays' load profiles, the historical load profiles were normalized according to (4). The normalized daily load profile was determined by dividing the hourly electricity load by the sum of that day, such that the integral of the normalized profile for each day becomes 1 [31].

$$V_t = P_t / \sum P_t \tag{4}$$

TABLE 4. List of korean holidays.

Calendar	Holiday	Label	Range of Gregorian dates (Lunar date)
S	New Year's Day	NFD	Jan 1
L	Lunar New Year (*Seollal*)	LN1~3	LN1: Jan 22 ~ Feb 18 (Dec 31) LN2: Jan 23 ~ Feb 19 (Jan 1) LN3: Jan 24 ~ Feb 20 (Jan 2)
S	Korean Independence Movement Day	IMD	March 1
S	Labor Day	LBD	May 1
L	Buddha's Birthday	BDD	May 3 ~ May 28
S	Children's Day	CHD	May 5
S	Korean Memorial Day	KMD	Jun 6
S	Korean Independence Day	KID	Aug 15
L	Korean Thanksgiving (*Chuseok*)	KT1~3	KT1 : Sep 7 ~ Oct 3 (Aug 14) KT2 : Sep 8 ~ Oct 4 (Aug 15) KT3 : Sep 9 ~ Oct 5 (Aug 16)
S	National Foundation Day [a]	NFD	Oct 3
S	Hangul Day	HGD	Oct 9
S	Christmas Day	CHR	Dec 25
S	Election Day	ELD	Not fixed [b]

[a] If the National Foundation Day is included in Korean Thanksgiving Day (KT1~KT3), it is treated as Korean Thanksgiving Day.
[b] The date of Election Day is not fixed but is usually the first or second Wednesday of April, May, or June. In this paper, various election events in the past ten years are regarded as the same election day except for the presidential election held in December.

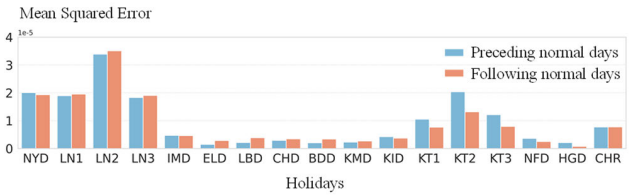

FIGURE 5. Mean squared error (MSE) of the normalized load pattern between holidays and the normal days preceding and following the holidays for one week. The data cover ten years from 2010 to 2019.

Fig. 5 presents the mean squared error of the daily normalized load patterns between holidays and the nearest normal days that precede or follow each holiday. The normal days that are parsed to calculate dissimilarities with the target holiday have the same DOW as the target holiday. In addition, some holidays (NYD, LN1–LN3, and KT1–KT3) show relatively high dissimilarity with the normal days preceding and following them. Therefore, they are not likely to follow a typical load pattern based on their DOW; rather, they follow their unique patterns. It is concluded that two calendar attributes–holiday type and DOW–affect load profiles of holidays. Based on their characteristics of load patterns, holidays can be classified into the following categories:

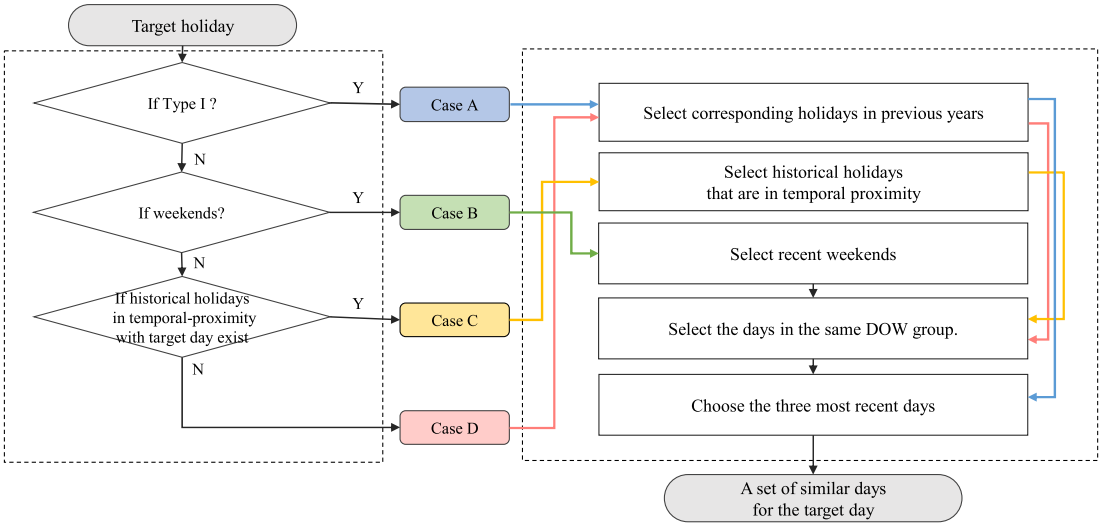

FIGURE 6. Framework of rule-based similar day selection module.

TABLE 5. Comparison of the ratio (%) of electricity consumption.

Mon	Tue	Wed	Thu	Fri	Sat	Sun
92.4	92.8	92.6	94.6	89.9	99.8	98.6

TABLE 6. Average first difference of hourly scaled weather features.

	TA	HM	SI	RN	CC	WS
Observation	0.0123	0.0330	0.0480	0.0046	0.0999	0.0429
Forecast	0.0118	0.0282	0.0477	0.0028	0.0245	0.0214

(1) Type I holidays: The load pattern follows their holiday-type characteristics.
(NYD, LN1∼LN3, and KT1∼KT3)
(2) Type II holidays: The load pattern follows their DOW characteristics.
(IMD, ELD, LBD, CHD, BDD, KMD, KID, NFD, HGD, and CHR)

Table 5 shows the ratio of the daily electricity consumption of holidays and the average electricity consumption of normal days in the previous three weeks with the same DOW as the holiday. In general, electricity consumption on holidays considerably decreases compared to that of normal days (up to 10.1 %p), but when holidays fall on weekends, no significant decrease is recorded (up to 1.4 %p). It can be inferred that weekends close in time to the target holidays show similar levels of electricity load consumption. If the target holiday is a Type II holiday and falls on weekends, its load profile might be similar to that of recent weekends.

Some Type II holidays are in temporal proximity with each other. Referring to Table 6, Labor Day, Children's Day, and Buddha's Birthday are all held in May. Likewise, National Foundation Day and Hangul Day are both in early October, showing similar load patterns if they are in the same DOW group. The indicated characteristics of holidays' load profiles are summarized as follows:

(1) A load profile of a holiday follows either a typical pattern of its DOW or a unique intraday pattern according to its holiday type.

(2) If a Type II holiday falls on a weekend, its daily load consumption is similar to that of the recent normal weekends.

(3) The load profiles of Type II holidays which are in temporal proximity share similar patterns and levels according to their DOW group.

2) RULE-BASED SIMILAR DAY SELECTION

In this study, a similar day is defined as a day with similar calendar attributes to the target holiday and is considered a similar calendar day. Therefore, the remaining weather and trend effects can be isolated. In this paper, a similar day selection (SDS) module employing a rule-based selection algorithm has been proposed. The overall operation of the SDS selection module is shown in Fig 6. Based on the three characteristics of holidays' load profiles, the SDS module classifies four selection cases from three conditional statements. Once the selection case is determined, the most recent three days that satisfy the conditions for each case are finally selected as similar days. The three sets of candidates of similar days are listed as follows: 1) corresponding holidays in preceding years, 2) recent weekends, and 3) other holidays in temporal proximity. A mechanism to select holidays in temporal proximity with the target holiday has been proposed to optimize the historical load profiles. The two benefits of including holidays in temporal proximity as candidates of similar days are as follows: 1) more recent data can be utilized, and 2) the shortage of corresponding holiday data can be overcome.

Case A: For Type I holidays, similar days were selected based on the rule of Case A. Since Type I holidays follow their unique load patterns, their similar days are selected from

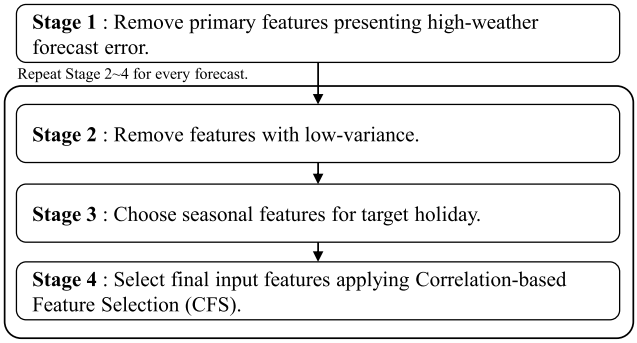

FIGURE 7. Four stages of the weather feature selection module.

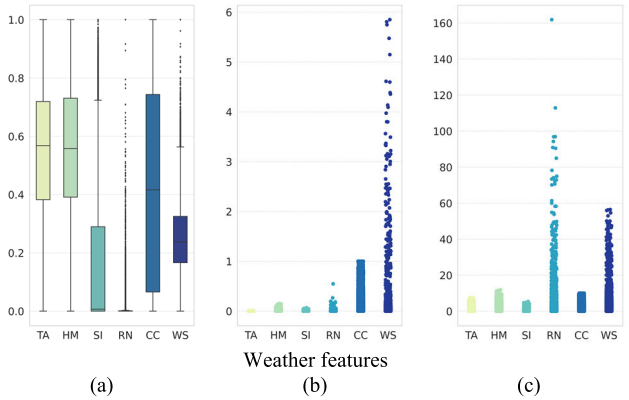

FIGURE 8. (a) Boxplot of the observed primary weather features from January 1, 2017, to December 31, 2019. (b) Squared forecast error of the primary weather features from January 1, 2017, to December 31, 2019. (c) Absolute scaled error of the primary weather features from January 1, 2017, to December 31, 2019.

the corresponding holidays in preceding years regardless of their DOW group.

Case B: For Type II holidays that fall on weekends, the most recent three days of the same DOW were selected as similar days.

Case c: In this case, the target holiday is a Type II holiday, which is nearer to other holidays. The candidates of similar days include the corresponding holidays of preceding years and other holidays in temporal proximity. Among these candidates, the most recent three days that are in the same DOW group with the target holiday are selected as similar days.

Case D: In this case, the target holiday is a Type II holiday, and no other holidays in temporal proximity exist. Thus, the candidates of similar days are the corresponding holidays of preceding years. Among these candidates, the most recent three days that are in the same DOW group with the target holiday are selected as similar days.

C. SELECTING INPUT WEATHER FEATURES

Through the weather feature selection (WFS) module, a set of input weather features is determined by selecting some features among a total of 20 weather features from the dataset. The weather dataset includes various weather features; however, the use of only a subset of input weather features by removing features irrelevant to the target and redundant to other features is more efficient. In this section, the proposed procedure of feature reduction and selection to effectively estimate the weather-induced load demand is illustrated. This procedure follows four stages as shown in Fig. 7. In Stage 1, the primary weather features that have low compatibility between observation and forecast are removed. Then, the following three stages are performed for the remaining weather features for each target holiday; thus, the overall stages can adaptively determine the set of input weather features.

1) WFS: STAGE 1. REMOVE PRIMARY FEATURES WITH POOR ACCURACY

In Stage 1, the observed/forecasted primary weather data are analyzed to measure their correspondence. Each weather feature has a different unit, as presented in Table 3. Weather features are scaled in the range [0,1] based on the observed weather data according to (5) to make them scale-free and to analyze their distribution.

$$W_t = \frac{W_t - W_{min}}{W_{max} - W_{min}} \tag{5}$$

This study focuses on the distribution of scaled weather features and weather forecasting errors to evaluate the compatibility and usefulness of each feature. Moreover, it is essential to evaluate the primary weather features because weather forecast errors can lead to load forecasting errors. Fig. 8 (a) presents a boxplot of the scaled value of observed weather features for the recent three years (2017-2019). Each horizontal line of the boxes represents the quartile of the feature, and dots represent the outliers using the interquartile range (IQR) rule.

As shown in Fig. 8 (a), the ratio of outliers in RN is exceptionally high (20.05%) compared to other features, especially compared to the SI, which has the second-highest (3.29%) ratio of outliers. Given that the distribution of precipitation values is concentrated at 0 because most of the rain falls intensively during a specific period, it can be said that the RN has high kurtosis. This can lead to poor estimation of weather sensitivity because of the biased distribution of features. Fig. 8 (b) shows a scatter plot of the squared forecast error of the scaled primary weather features. Besides, the forecast error of WS is extraordinarily high and variant. Given that all features are scaled into a range of 0 to 1, the forecast of CC also presents a substantially high error. It can be inferred that the forecasts and observations for WS and CC are not compatible. Fig. 8 (c) shows the absolute scaled error (ASE) of the primary weather features. The ASE is an accuracy metric of forecasts that is independent of the scale of the data. According to (6), it is defined as the difference between a forecast and an observation divided by the average one-step naive forecast computed in-sample. It can replace the mean absolute percentage error (MAPE), which is likely to produce infinite values due to division by zero [32]. The scaled

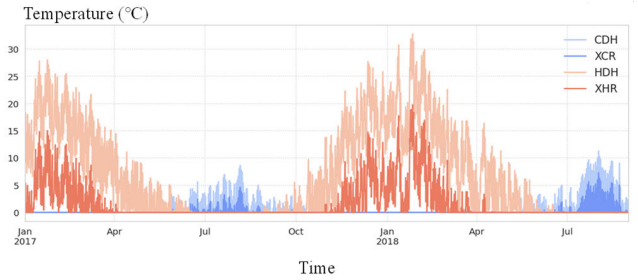

FIGURE 9. Plot of low-variance features—CDH, HDH, XCR, XHR. CDH and XCR show quasi-constant values in winter and so do HDH and XHR in summer.

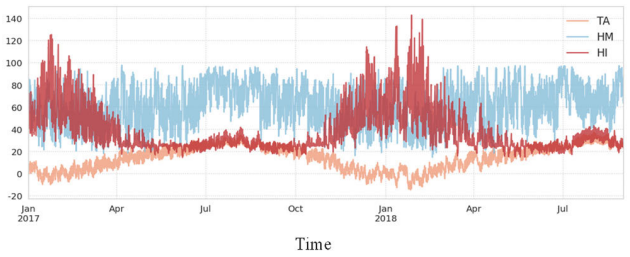

FIGURE 10. Dry-bulb temperature, relative humidity, and heat index. While heat index is a weather feature to show the complex effect of dry-bulb temperature and relative humidity, it shows a larger value in winter than in summer.

weather features can have zero values; therefore, an ASE is adopted to evaluate the forecast accuracy. In Fig. 8 (c), both RN and WS show a high and variant ASE.

$$ASE_t = \left| \frac{e_t}{\frac{1}{n-1} \times \sum_{i=2}^{n} |Y_i - Y_{i-1}|} \right| \tag{6}$$

Table 6 shows the average absolute value of the first difference for both the hourly observation and forecast of primary weather features. The first difference values of the observation and forecast of RN, CC, and WS are very different from each other. Three primary weather features (RN, WS, and CC) exhibit the following characteristics: high-kurtosis, high forecasting error, and inferior correspondence between the observed and forecasted data. Thus, in this study, these three primary features were removed from the set of input features.

2) WFS: STAGE 2. REMOVE THE FEATURES WITH LOW VARIANCE

Fig. 9 shows that some weather features, especially temperature-derived features (CDH, HDH, XCR, and XHR), are quasi-constant during a specific period. They are introduced to reflect the cooling and heating load consumption and occur only when the dry temperature is higher or lower than a specific value. This means that these features have a variance close to zero when the dry-bulb temperature value does not meet such conditions. Features with low variance are assumed to have no effect on the load demand and are included in the final set of input weather features based on their variance. For example, HDH and XHR do not affect the load profile during the days of midsummer, and neither does CDH and XCR during the days of winter. Therefore, in Stage 2, weather features with a variance lower than a predetermined small variance threshold were filtered out.

3) WFS: STAGE 3. SELECT SECONDARY FEATURES ADAPTIVELY

Certain weather features are valid only for a specific period. Since secondary weather features are created by combining or transforming primary features, their physical characteristics that are related to the load demand are considered. Fig. 10 shows that the heat index becomes a humidity-dependent variable when the temperature is considerably low. Although the heat index was introduced to measure the combined effect of relative humidity and air temperature, its value is higher in winter than in summer. This is because simple mathematical calculations based on formulas can produce irrational results. Thus, secondary weather features must be selected adaptively depending on the target holiday. KMA provides the forecast value of "discomfort index" and "heat index" only for 4 months from July to September. In addition, the "windchill" forecast is available for only 5 months, from November to March. Referring to KMA, three weather features (DI, HI, and WC) are selected only if the target holiday is included in the period depicted above.

4) WFS: STAGE 4. APPLICATION OF CFS

The WFS procedures select features that involve two characteristics: 1) relevance to the target feature and 2) not being redundant with the other weather features. Thus, a correlation-based feature selection (CFS) approach is considered for determining the input features of the proposed model. The CFS uses a correlation-based heuristic as a metric to evaluate the goodness of features [33]. By adopting the CFS approach, the number of features can be reduced, and "multicollinearity" can be prevented. The CFS approach considers the correlation coefficients of feature-to-output and feature-to-feature. The original CFS method adopts a heuristic to evaluate a subset of features as follows:

$$Merit_S = \frac{k\bar{r_{cf}}}{\sqrt{k + k(k-1)\bar{r_{ff}}}}, \tag{7}$$

where

k : number of features in S;
$\bar{r_{cf}}$: average feature class (target) correlation;
$\bar{r_{ff}}$: average feature–feature intercorrelation.

Starting with an empty set, a search strategy (usually the best-first searching algorithm) expands a feature subset by adding a single feature and finally chooses the best subset of features. However, when the original heuristic expressed in (7) was applied, either an extremely high or extremely low number of features was selected. Thus, in this study, only the main idea of the CFS approach was adopted by considering features that were highly correlated to the target and removing those that were highly intercorrelated with each

other. The process of the proposed WFS method is presented in Algorithm 1.

Algorithm 1 : Stage 4 - WFS Algorithm

Input: *RLD (Reconstituted load)*
$W_{init} = \{wt_x | \rho_{RLD,wt_a} \geq \rho_{RLD,wt_b}, (1 \leq a \leq b \leq N)\}$
(A set of weather features)
Output: W_{input} *(A set of input weather features)*
Initialize: $k \leftarrow 1$; $W_{input} \leftarrow \emptyset$; $W_{removal} \leftarrow \emptyset$;
while $k \leq N$ **do**
  $G_k = \{wt_x | \rho_{wt_x,wt_k} \geq threshold, k < x \leq N$
  if $\boldsymbol{wt_k \notin D}$ **then**
    $W_{input} \leftarrow W_{input} \cup \{wt_k\}$
    $W_{removal} \leftarrow W_{removal} \cup G_k$
  else
    pass
  end
    $k \leftarrow k + 1$
end

The proposed WFS method is a simple and fast "rank-and-select" method. First, the total N weather features are ranked according to the correlation coefficient with the target feature (load demand) from the first to the N-th features. Two empty sets were initially defined for features that include the selected features (W_{input}) and removed features ($W_{removal}$). The weather feature searching process is performed iteratively in the order of the ranking of each feature. For the k-th weather feature, wt_k, a set G_k of features highly correlated with wt_k is determined by a predefined threshold value (0.8). If wt_k has not yet been included in W_{input} and $W_{removal}$, then wt_k is added to W_{input} and all elements of G_k are added to $W_{removal}$. Finally, after the searching process is over, W_{input} has features that are highly correlated with the target value, and $W_{removal}$ has features that are highly correlated with the features included in W_{input}.

D. FORECASTING BASED ON LOAD MODIFICATION BY WTSM

After selecting similar days and determining a set of input weather features for the target holiday, in this module, weather-induced load between a similar day and target holiday is estimated using WTSM according to the following procedures:

Step 1: Determine a WTSM for a pair of the target holiday and a similar day.

Step 2: Produce a modified load profile for a similar day by applying a "load modifying function" that takes WTSM as an input argument.

Step 3: Make a final load forecast by calculating the weighted average of the modified load profile for each similar day obtained from Step 2.

A four-dimensional matrix WTSM, $\boldsymbol{M_{i,j}}$ for target holiday and similar day, was defined by concatenating four matrices, as shown in (8). $\left[\boldsymbol{TH_{i,j}}(t,w)\right]$ is a "threshold matrix", and $\left[\boldsymbol{WTS_{i,j}}(t,w)\right]$ is a "sensitivity matrix". As presented in (9) and (10), each matrix is a two-dimensional array whose rows and columns represent "time slot" and "weather feature," respectively. The parameter t indicates "time slot," and a parameter w indicates each "weather feature," which is an element of a set of input weather features, W_{input}. A time slot t is defined as a section divided into equal intervals for 24 h per day. Therefore, t_h is defined as the time slot at hour h. A threshold matrix contains the value of weather data and can determine the applicability of the weather sensitivity matrix. In weather-sensitive seasons, the electric load responds to changes in weather, but under certain weather conditions, it may be insensitive. This means that the electric load does not respond monotonically to changes in weather. Thus, a threshold matrix is introduced to reflect this nonlinearity between the load and weather. A sensitivity matrix contains the value of load-weather sensitivity for each weather feature. The load-weather sensitivity varies over time; thus, the response of the load demand to changes in weather conditions is not consistent over time. In this study, a total number of time slots was considered as $T = 4$.

$$\boldsymbol{M_{i,j}} = \begin{bmatrix} [\boldsymbol{TH}_{i,j}^{upper}(t,w)] & [\boldsymbol{WTS}_{i,j}^{upper}(t,w)] \\ [\boldsymbol{TH}_{i,j}^{lower}(t,w)] & [\boldsymbol{WTS}_{i,j}^{lower}(t,w)] \end{bmatrix} \tag{8}$$

$$\left[\boldsymbol{TH_{i,j}}(t,w)\right] = \begin{bmatrix} TH_{i,j}(1,w_1) & \cdots & TH_{i,j}(1,w_N) \\ \vdots & \ddots & \vdots \\ TH_{i,j}(T,w_1) & \cdots & TH_{i,j}(T,w_N) \end{bmatrix} \tag{9}$$

$$\left[\boldsymbol{WTS_{i,j}}(t,w)\right] = \begin{bmatrix} WTS_{i,j}(1,w_1) & \cdots & WTS_{i,j}(1,w_N) \\ \vdots & \ddots & \vdots \\ WTS_{i,j}(T,w_1) & \cdots & WTS_{i,j}(T,w_N) \end{bmatrix} \tag{10}$$

Taking WTSM as one of the input arguments, the load-modifying function f is defined as shown in (11). It takes several arguments related to two time periods, i(in this case, a similar day) and j(in this case, a target holiday), and outputs the array of modified load for 24 h ($\boldsymbol{MLoad}_{i,j}$).

$$f : \boldsymbol{MLoad}_{i,j} = f \begin{pmatrix} \boldsymbol{M_{i,j}}, \\ GR_i^j, \\ \boldsymbol{RLoad}_i, \\ \boldsymbol{WT}_j^{fcst}, \\ \boldsymbol{WT}_i^{obs}, \\ \boldsymbol{SOL}_j \end{pmatrix} \tag{11}$$

$$\boldsymbol{MLoad}_{i,j} = \left[MLoad_{i,j}(h)\right] \tag{12}$$

$$\boldsymbol{RLoad}_i = [RLoad_i(h)] \quad (\mathrm{h} = 0, 1, \cdots, 23) \tag{13}$$

$$\begin{aligned} MLoad_{i,j}(h) = {} & GR_i^j \times RLoad_i(h) \\ & + \sum_{w \in S} \left\{ \left(WT_j^{fcst}(h,w) - WT_i^{obs}(h,w) \right) \right. \\ & \times \begin{pmatrix} WTS_{i,j}^{upper}(t_h,w) \times U(h,w) \\ + WTS_{i,j}^{lower}(t_h,w) \times L(h,w) \end{pmatrix} \\ & \left. - BTM_j(h) \right\} \end{aligned} \tag{14}$$

$$GR_i^j = \frac{\sum_{d=j-365days}^{j} \sum_{h=0}^{h=23} RLoad_d(h)}{\sum_{d=i-365days}^{i} \sum_{h=0}^{h=23} RLoad_d(h)} \quad (15)$$

$$U(h,w) = \begin{cases} 1 & if\ WT_j^{fcst}(t_h,w) > TH_{i,j}^{upper}(t_h,w) \\ 0 & otherwise \end{cases} \quad (16)$$

$$L(h,w) = \begin{cases} 1 & if\ WT_j^{fcst}(t_h,w) < TH_{i,j}^{lower}(t_h,w) \\ 0 & otherwise \end{cases} \quad (17)$$

where

GR_i^j : ratio of the total load consumption in the previous 365 days from *day j* and *dayi*;
$RLoad_i(h)$: reconstituted load on *dayi* at *hour* $= h$;
$WT_j^{fcst}(h,w)$: weather forecast of weather feature w at *hour* $= h$ on *day j*;
$WT_i^{obs}(h,w)$: weather observation of weather feature w at *hour* $= h$ on *day i*;
$WTS^{upper}(t_h,w)$: weather sensitivity value of weather feature w at *timeslot* $= t_h$ when $U(w,h) = 1$;
$WTS^{lower}(t_h,w)$: weather sensitivity value of weather feature w at *timeslot* $= t_h$ when $L(w,h) = 1$;
$BTM_j(h)$: BTM PV generation forecast at *hour* $= h$ on *day j*.

The hourly modified historical load of a similar day is obtained using (14) by incorporating four major factors. The BTM PV and calendar effect are incorporated by employing the reconstituted load method and similar day selection; thus, the remaining two major factors are isolated. The coefficient GR_i^j is multiplied by the historical hourly load profile to consider the yearly load demand increase. The summation term in (14) incorporates the effect of weather on the load profile. When the threshold conditions (16) and (17) are satisfied at hour h, the weather effect is incorporated by adding a weather-induced load. For the selected weather features, weather-induced load terms were added every hour. The forecasted BTM PV generation over hours is subtracted to forecast the net load of the target holiday. The problem P0 is designed to determine the optimal WTSM that minimizes the error rate (MAPE) between the modified load and real load, as shown in (18). $\boldsymbol{Avg}(\boldsymbol{X})$ returns the mean value of all elements in matrix $\boldsymbol{X}$, and $\boldsymbol{X}^{|*|}$ converts every element to its absolute value. The subscripts i and j denote similar days and target holidays, respectively.

$$\begin{aligned} \text{P0}: \min_{\boldsymbol{M}_{i,j}} & \ g_0\left(\boldsymbol{M_{i,j}},\right) \\ & g_0\left(\boldsymbol{M_{i,j}},\right) \\ = & \ \boldsymbol{Avg}\left(\left(\frac{\boldsymbol{MLoad}_{i,j} - \boldsymbol{Load}_j}{\boldsymbol{Load}_j}\right)^{|*|}\right) \\ = & \ \boldsymbol{Avg}\left(\frac{\mathbf{1}}{\boldsymbol{Load}_j}\left(f\begin{pmatrix}\boldsymbol{M_{i,j}},\\ GR_i^j,\\ \boldsymbol{RLoad}_i,\\ \boldsymbol{WT}_j^{fcst},\\ \boldsymbol{WT}_i^{obs},\\ \boldsymbol{BTM}_j\end{pmatrix} - \boldsymbol{Load}_j\right)^{|*|}\right) \end{aligned} \quad (18)$$

However, it is impossible to know the future real load of the target holiday, $\boldsymbol{Load}_j$, while performing load forecasting. Thus, the following two assumptions are made and an alternative approach is proposed to overcome this limitation.

Assumption 1: The set of input weather features related to the load is similar within a short period.

Assumption 2: The amount of change in the electricity demand in response to weather changes on one day is similar to that of the adjacent period.

Thus, the RP is introduced to utilize known data. It refers to the period that covers the preceding normal days adjacent to a specific day, as shown in Fig. 11. Each RP, Ref_i and Ref_j, illustrated in Fig. 11, has the same length (7 days) and consists of days in the same order. Based on the above two assumptions, $\boldsymbol{M_{i,j}}$, which is to be determined, is coupled with $\boldsymbol{M_{Ref_i,Ref_j}}$, which is the WTSM between Ref_i and Ref_j. For both RPs, weather, load profiles, and BTM PV generation data are available. Finally, f and g are related, and the optimization problem P1 is designed to determine the optimal WTSM in (19).

$$\begin{aligned} \text{P1}: \min_{\boldsymbol{M}_{Ref_i,Ref_j}} & \ g_1\left(\boldsymbol{M_{Ref_i,Ref_j}}\right) \\ & g_1\left(\boldsymbol{M_{Ref_i,Ref_j}}\right) \\ = & \ \boldsymbol{Avg}\left(\left(\frac{\boldsymbol{MLoad}_{Ref_i,Ref_j} - \boldsymbol{Load}_{Ref_j}}{\boldsymbol{Load}_{Ref_j}}\right)^{|*|}\right) \\ = & \ \boldsymbol{Avg}\left(\frac{\mathbf{1}}{\boldsymbol{Load}_{Ref_j}}\left(f\begin{pmatrix}\boldsymbol{M_{Ref_i,Ref_j}},\\ GR_i^j,\\ \boldsymbol{RLoad}_{Ref_i},\\ \boldsymbol{WT}_{Ref_j}^{fcst},\\ \boldsymbol{WT}_{Ref_i}^{obs},\\ \boldsymbol{BTM}_{Ref_j}\end{pmatrix} - \boldsymbol{Load}_{Ref_j}\right)^{|*|}\right) \end{aligned} \quad (19)$$

The GA, which is a search process based on the laws of natural selection and genetics, was adopted in this study to find an optimal $\boldsymbol{M_{Ref_i,Ref_j}}$ [34]. The key advantage of using a GA is in its computational efficiency. It is suitable for handling nonlinear objective functions and constraints for multiple decision variables. For the coupled problem P1, the objective function $g_1(\boldsymbol{M_{Ref_i,Ref_j}})$ is a nonlinear and non-differentiable function, and the number of decision variables, all elements of $\boldsymbol{M_{Ref_i,Ref_j}}$, is large. Other methods such as the least-square method and the gradient method often fail in the search if the model structure is not differentiable or

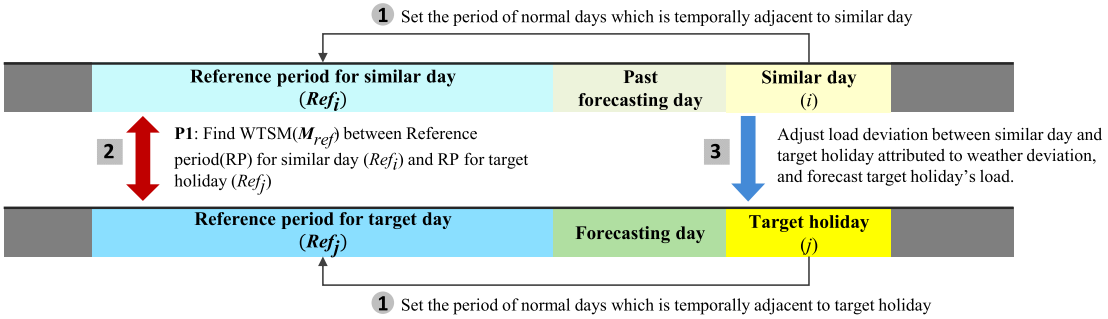

FIGURE 11. The reference periods for a target holiday and a similar day. They are introduced to design the alternative problem (P1).

linear in parameters [35]. The real-coded GA is implemented by employing the following steps:

Step1 (Initialization): Randomly generate the initial population with population size N_p.

Step2 (Evaluation of objective function for the initial population): Evaluate each chromosome in the initial population using objective function values.

Step3 (Copy): Copy and transfer the fittest chromosomes to the next generation by the elite ratio P_e.

Step4 (Selection): Select parents among the chromosomes of the current generation by the ratio of the parents' ratio $P_p$to reproduce the population of the next generation.

Step5 (Crossover): Produce a new generation by combining the parents selected from the *Selection* phase with the probability of P_c.

Step6 (Mutation): Replace the randomly selected original genes in each chromosome with random values using the probability of P_m.

Step7 (Evaluation of objective function): Evaluate each chromosome in the current population using objective function values.

Step8 (Termination condition check): Check if the termination condition is satisfied. If yes, terminate the iterative procedure.

Step9 (Repeat steps): If the termination condition is not satisfied, repeat Step3–Step8 until the termination condition is satisfied.

Conventionally, the termination condition ends the search when an upper limit on the number of generations is reached [36]. Once WTSM linked to a pair of similar day i and target holiday j has been determined as $\boldsymbol{M}^*_{i,j}$ through GA, the final value of the objective function is $v_i = g_1\left(\boldsymbol{M}^*_{i,j}\right)$. The daily load prediction results are generated for each selected similar day through (14). Weighted averaging was adopted to combine these results. Each weight for a modified similar day's load is determined based on the final value of the objective function, v_i. The weight of the modified load profile of similar day i is defined in (20).

$$u_i = \frac{1/v_i}{\sum_{l=1}^{N_s} 1/v_l}, \tag{20}$$

where

u_i : combination weight for a similar day i;
v_i : the final value of the objective function of GA for a similar day i;
N_s : number of similar days for the given target holiday

Finally, the forecasted daily net load profile of a given target holiday is expressed as follows:

$$NetFcstLD(h) = \sum_{l=1}^{N_s} u_l \times MLoad_{l,j}(h) \tag{21}$$

IV. CASE STUDY

In this section, the proposed method is compared to three benchmarks—the fuzzy linear regression, XGBoost, and LSTM. They were tested on holidays in 2018 and 2019. The fuzzy linear regression has been adopted as a method for short-term load forecasting on holidays by KPX, the ISO of Korea. MAPE and RMSE were used as the evaluation metric for accuracy; it is expressed as follows.

$$\text{MAPE} = \frac{1}{H}\sum_{h=1}^{H}\left|\frac{\hat{Y}_h - Y_h}{Y_h}\right| \times 100(\%), \tag{22}$$

$$\text{RMSE} = \sqrt{\frac{1}{H}\sum_{h=1}^{H}(\hat{Y}_h - Y_h)^2}, \tag{23}$$

where

$\hat{Y}_h$: forecasted load at hour h (MW);
Y_h : actual load at hour h (MW);
H : forecasting time horizon (hours)

The details of the GA parameters applied to the proposed method are illustrated in Table 7.

TABLE 7. Parameters of the genetic algorithm.

Parameter name	Value
Crossover type	convex crossover [37]
Maximum iterations	1000
Elite ratio (P_e.)	0.1
Parents ratio (P_p)	0.3
Crossover probability (P_c)	0.5
Mutation probability (P_m)	0.1

The schemas in the datasets used in this case study are described in Table 8.

TABLE 8. Description of datasets: The starting point of acquired data.

Schema	Observed	Forecasted
Load profiles	2009/12/01	-
Weather	2009/12/01	2013/01/01
BTM PV generation	2015/01/01	2015/01/01

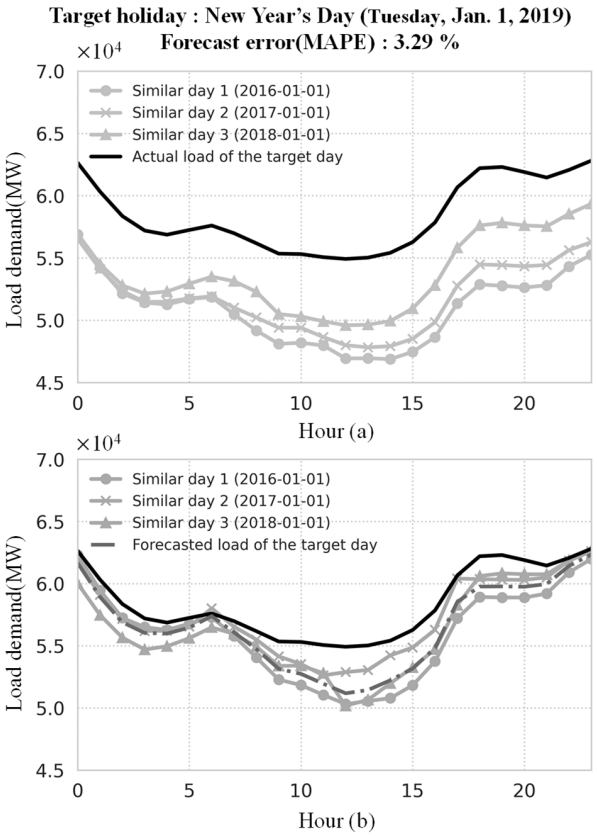

FIGURE 12. Load forecasting for New Year's Day (Tuesday, Jan. 1, 2019). (a) Actual load profiles of similar days and the target holiday. (b) Predictions from each similar day and the forecasted load of the target holiday.

Holiday load forecasting was performed for New Year's Day (Type I holiday) and Korean Independence Day (Type II holiday) in 2019 for 24 h using the proposed method. Both holidays fall in the weather-sensitive season (winter and summer).

New Year's Day is a Type I holiday; therefore, according to the rule illustrated in Fig. 6, the corresponding holidays of the preceding years are selected as similar days. Fig. 12(a) shows the actual load profiles of the target holiday and similar days. They share similar intraday load patterns, but their daily energy consumption differs. Fig. 12(b) shows the modified load of each selected similar day and the final forecasted net load, which is the weighted sum of the modified loads. These values converged to the actual load profile of the target holiday, and the forecasting error (MAPE) was 3.29%. Through the WFS module, four weather features were selected for the target holiday. Fig. 13 shows the scaled

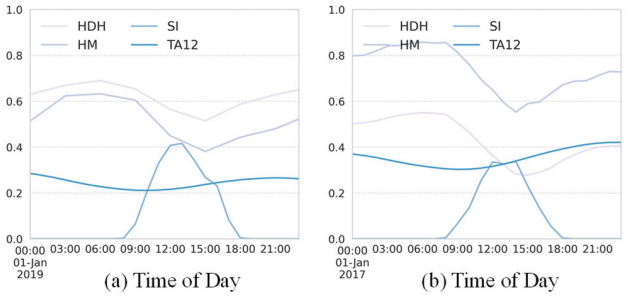

FIGURE 13. Weather-induced load between (a) the target holiday (Jan. 1, 2019) and (b) the similar day (Jan 1, 2017).

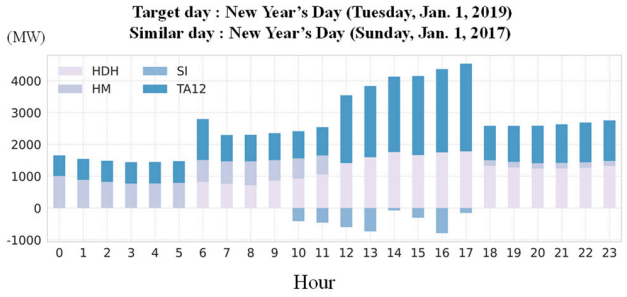

FIGURE 14. Weather-induced load between the target holiday (Jan. 1, 2019) and the similar day (Jan. 1, 2017).

weather forecast and observation of a pair of the target and similar days. The overall temperature and relative humidity of the target holiday were lower than those of a similar day. This can lead to a higher heating load and less lighting load on the target holiday. Fig. 14 presents the hourly weather-induced load of New Year's Day due to different weather conditions between the target holiday and a similar day. Given the positive weather-induced load caused by the difference in HDH and TA12, it can be inferred that the proposed method estimated the weather effect correctly.

Since Korean Independence Day falls in the weather-sensitive season, its load forecast error rate is usually high. In addition, the heatwave period and rainy season in summer may likely overlap within this day, and a continuous and cumulative effect of high temperature can occur. Figs. 15(a) and (b) show the case of load forecasting on Korean Independence Day in 2019. According to the SDS rule, corresponding holidays in the same DOW group are selected as similar days. Fig. 15(b) shows the modified load profiles of the selected similar days. The forecasting error of the proposed method was 2.30%. Fig. 16 shows that the similar day was cooler and rainier than the target holiday; therefore, the weather conditions of these days were different. It can be inferred that fewer cooling requirements and more lighting load on the target holiday occurred. Fig. 17 shows the weather-induced load between the target holiday and one of the similar days and reveals that the decrease in the load demand was induced by the difference in dry-bulb temperature, temperature averaged over 24 h, wet-bulb

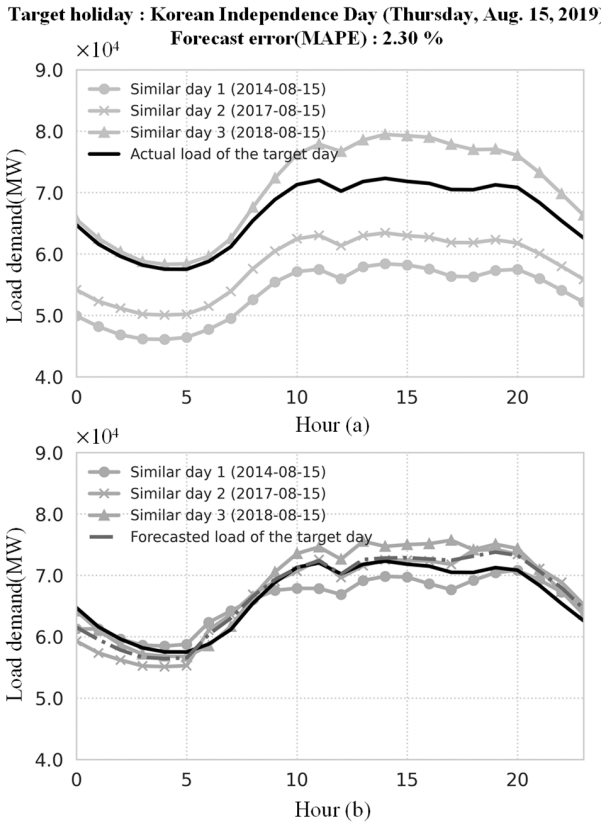

FIGURE 15. Load forecasting for Korean Independence Day (Thursday, Aug. 15, 2019). (a) Actual load profiles of the similar days and the target holiday. (b) Predictions from each similar day and the forecasted load of the target holiday.

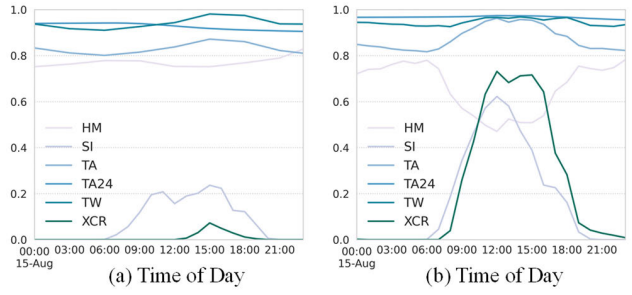

FIGURE 16. Weather-induced load between (a) the target holiday (Aug. 15, 2019) and (b) the similar day (Aug. 15, 2018).

temperature, extra-cooling requirements, and humidity between the similar day and the target holiday.

It took approximately 9,313 s to forecast the load demand on holidays subject to the case study, and it was found that it takes 282 s on average for each holiday. The results were obtained on a PC with Intel Xeon 16Core (2.1Ghz) and 128 GB RAM. Table 9 shows the forecasting errors of the proposed method and fuzzy linear regression.

The proposed method in Table 9 shows that the average annual MAPE in 2018 and 2019 was 1.76% and 2.62%, respectively, improving forecasting accuracy in comparison

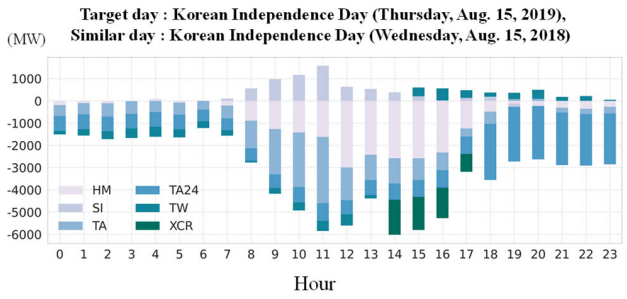

FIGURE 17. Weather-induced load between the target holiday (Aug. 15, 2019) and the similar day (Aug. 15, 2018).

TABLE 9. Holiday load forecasting results: MAPE (%).

Holiday	Proposed method		Fuzzy linear regression		LSTM		XGBoost	
	MAPE (2018)	MAPE (2019)	MAPE (2018)	MAPE (2019)	MAPE (2018)	MAPE (2019)	MAPE (2018)	MAPE (2019)
NYD	2.53	3.29	5.30	3.36	5.79	5.25	5.18	3.39
LN1	0.88	4.68	2.49	1.65	12.77	17.82	3.65	8.90
LN2	1.15	3.26	1.61	1.55	10.52	14.55	2.07	8.19
LN3	0.89	3.62	1.18	3.91	3.56	3.31	4.88	6.77
IMD	2.47	4.73	2.17	5.14	12.17	5.57	2.40	5.05
BDD	1.57	1.60	7.05	2.16	2.78	4.07	3.37	4.41
LBD	0.66	2.39	3.28	3.54	1.43	3.04	6.77	5.49
CHD	3.48	1.52	2.95	3.12	4.00	1.44	5.14	5.68
KMD	2.99	2.08	2.44	0.88	3.56	6.34	2.87	8.81
IND	3.23	2.30	5.60	6.20	5.60	3.64	3.69	9.65
KT1	1.64	2.52	0.99	4.00	7.97	16.92	18.85	15.13
KT2	1.05	2.54	0.84	5.22	11.35	18.59	11.42	8.63
KT3	0.88	2.86	1.22	4.36	7.09	12.89	4.45	6.30
NFD	1.31	1.91	2.74	3.97	2.52	7.35	5.91	11.72
HGD	1.17	0.79	2.24	7.95	1.58	2.31	3.39	31.07
CHR	2.56	1.76	3.19	1.84	1.44	2.89	12.05	17.15
ELD	1.43	-	3.46	-	4.89	-	4.97	-
AVG.	1.76	2.62	2.87	3.68	5.82	7.87	5.94	9.77

TABLE 10. Holiday load forecasting results: RMSE (MW).

Holiday	Proposed method		Fuzzy linear regression		LSTM		XGBoost	
	RMSE (2018)	RMSE (2019)	RMSE (2018)	RMSE (2019)	RMSE (2018)	RMSE (2019)	RMSE (2018)	RMSE (2019)
NYD	1607.17	2158.90	3006.76	2362.49	3593.76	3909.43	3321.23	2387.27
LN1	1858.91	2873.72	1639.39	3495.64	7354.02	10094.36	2985.81	5513.43
LN2	487.48	1510.27	1919.59	2119.57	5239.33	6974.33	1347.22	5300.03
LN3	2038.48	850.04	1603.22	1736.66	2153.88	2066.43	2812.80	3465.46
IMD	2027.35	1411.83	1611.72	687.78	7741.60	3843.81	1650.11	3034.83
BDD	2633.18	1731.62	4552.95	4529.41	1717.06	2370.81	2828.50	3881.16
LBD	842.86	1477.25	1710.90	2511.26	982.51	1927.49	3995.12	3498.92
CHD	705.27	627.99	1570.08	5072.57	2467.71	879.67	3382.73	3183.12
KMD	1838.96	1225.43	2412.47	1353.71	2236.72	3924.98	2010.94	5691.52
IND	588.97	2701.61	1373.24	1052.03	4469.43	3025.64	2217.91	4975.45
KT1	622.66	2014.11	1037.67	886.43	3835.65	8769.30	9059.26	7155.70
KT2	534.23	2102.23	750.29	1988.54	4915.61	8294.26	6136.10	4641.94
KT3	962.59	1011.73	4523.16	1281.37	3343.56	6114.97	2608.79	3231.11
NFD	1021.97	1535.83	530.32	2096.99	1763.34	4580.85	2785.07	6200.56
HGD	525.51	1328.15	411.77	2256.16	1284.18	1556.95	1841.04	13518.35
CHR	466.09	1626.10	565.34	2070.45	1107.98	1981.40	5469.68	8138.42
ELD	1014.42	-	2487.78	-	3138.84	-	3181.54	-
AVG.	1163.30	1636.68	1865.10	2218.82	3373.25	4394.67	3390.23	5238.58

with benchmarks models. Specially, compared to the fuzzy linear regression, which is the benchmark model with the best forecasting accuracy, the decreases in the MAPE

TABLE 11. Holiday load forecasting results: Variance of hourly MAPE.

Holiday	Proposed method		Fuzzy linear regression		LSTM		XGBoost	
	VAR (2018)	VAR (2019)	VAR (2018)	VAR (2019)	VAR (2018)	VAR (2019)	VAR (2018)	VAR (2019)
NYD	2.44	3.64	4.09	6.46	16.51	22.62	16.61	6.61
LN1	0.39	6.66	0.61	1.51	45.58	123.40	10.74	11.67
LN2	0.54	5.66	1.71	2.01	19.91	36.74	1.78	36.58
LN3	0.41	5.55	0.70	0.95	5.68	7.47	7.36	10.18
IMD	3.11	2.24	1.92	10.37	5.55	12.84	2.00	3.61
BDD	0.45	2.10	14.74	2.28	1.99	5.61	3.30	11.88
LBD	0.35	2.71	1.55	4.28	1.22	4.60	4.00	5.40
CHD	4.33	0.72	1.27	4.49	7.90	1.31	7.01	4.50
KMD	2.42	1.59	1.58	0.50	1.86	5.14	2.02	14.43
IND	2.22	1.78	5.27	6.25	4.99	6.90	4.69	8.34
KT1	2.59	3.81	0.33	3.25	6.18	47.72	18.51	38.80
KT2	0.60	4.24	0.32	2.96	14.78	75.22	24.50	19.71
KT3	0.46	4.80	0.38	4.31	17.13	41.29	2.95	7.46
NFD	0.81	3.46	2.48	2.95	3.36	12.99	1.53	30.32
HGD	0.34	0.72	2.30	23.00	2.48	3.25	10.46	126.06
CHR	2.46	1.25	4.58	2.00	1.08	2.84	38.58	58.53
ELD	0.99	-	6.08	-	3.88		5.23	-
AVG.	1.47	3.18	2.94	4.85	9.42	25.62	9.49	24.63

values are approximately 1.11%p and 1.06%p in 2018 and 2019. Table 10 shows the RMSE comparison values using 2018 and 2019 data. The proposed method in this table shows a significantly smaller RMSE value compared to the benchmark models. These results prove that the proposed model is excellent not only in prediction accuracy but also in prediction precision. The prediction accuracy of LSTM and XGBoost models is lower compared to other models. It is presumed to be due to the limitation of the amount of training data depending on the characteristics of holidays that lack past data. In particular, such a phenomenon is well confirmed on holidays (LN1-3, KT1-3) following the lunar calendar.

Table 11 shows the variance of the hourly MAPE, a metric used to evaluate the stability of the forecasting accuracy. A small variance of the hourly forecast error means that the intraday patterns of the predicted load profiles and real profiles are consistent. The proposed method showed a smaller overall variance than the other benchmark models. This implies that the hourly pattern of the load forecasting result of the proposed method is consistent with that of the actual load profile.

To verify the effectiveness of the proposed method, three variations of the proposed framework were created, and their performance was each evaluated using the MAPE. A description of each variation is as follows.

1) V1: A model that reflects only the trend, calendar, and BTM PV effect. This model adopts all three modules in the proposed framework, while all elements of the WTSM are applied to load modification that is equal to zero, so the weather-induced load is ignored.
2) V2: A model that reflects the trend, calendar, BTM PV, and weather effect. This model adopts all three modules in the proposed framework, while not any combination method of the modified similar days' load profiles is applied.
3) V3: A model that reflects the trend, calendar, BTM PV, and weather effect. This model adopts all three modules in the proposed framework whereas a simple mean method is applied for combining the modified similar day's load profiles.
4) V4: A model that reflects the trend, calendar, BTM PV, and weather effect. In addition, it adopts all three modules in the proposed framework, and the combination method based on weighted average is applied to it. V4 equals the final framework proposed in this paper.

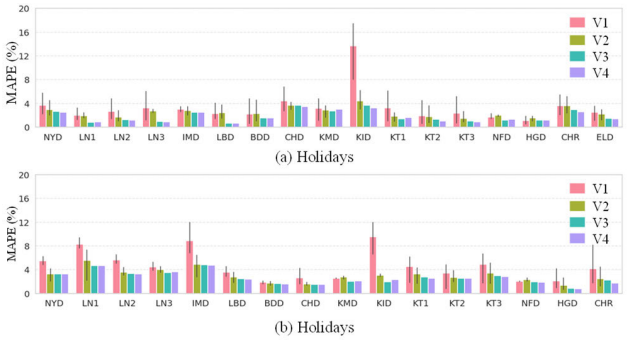

FIGURE 18. Graphical comparison of load forecasting error (MAPE) for holidays in (a) 2018 and (b) 2019 for the proposed framework (V4) and its variations (V1∼V3). The yearly average value of MAPEs of V3 is 1.83% in 2018 and 2.67% in 2019. As shown in Table, the yearly average value of MAPEs of the proposed framework is 1.76% in 2018 and 2.62% in 2019.

Figs. 18 (a) and (b) show the MAPE for holidays in 2018 and 2019, respectively. In the case of V1 and V2, the height of the bars of Fig. 18 is the average value of the MAPEs comparing the actual net load with the similar days' modified load profiles. The vertical lines represent their confidence interval. V1 had a larger mean of the MAPEs than V2, because V1 does not consider weather effects in forecasting. Judging from the fact that the confidence interval of the MAPEs of V2 is smaller than that of the V1, which means that the modified load profiles converge together, it can be inferred that the proposed framework effectively reflects weather effect by including various weather features and selecting input weather features. The combining methods are adopted to V3 and V4; thus, the height of the bars stands out of the MAPE of the final load forecast results. As shown in Fig. 18, V4 had the best performance. Furthermore, by comparing the yearly mean value of the MAPEs between V3 and V4, it can be concluded that the performance of load forecasting has been improved in both years by applying the proposed combining method.

V. CONCLUSION

In this study, a framework for holiday load forecasting that integrates four significant factors, calendar, trend, weather, and BTM PV, was proposed. The main idea of the proposed framework was to forecast a target holiday by modifying historical load profiles of similar days and combining them. A rule-based SDS module was introduced to reflect the

calendar effect. An adaptive WFS was introduced into the proposed framework to determine a set of input weather features. The mathematical model adopting a load modifying function was designed to integrate the trend and weather effect. For the quantification of weather-induced load, a WTSM was defined and determined by GA. Compared with the traditional fuzzy linear regression method, the proposed method achieves better forecasting accuracy with a yearly averaged MAPE of 1.76% and 2.62% for Korean holidays in 2018 and 2019, respectively. Furthermore, the results show that the proposed method is stable, given the fact that the variance of the forecasting error is low.

The extension of the proposed framework can be applied to day-ahead load forecasting for holidays to enhance forecasting accuracy. First, the described method of selecting weather features based on the analysis of the collected weather data can be a used as a guide to determine a set of input weather features. Second, the introduction of the WTSM used to reflect nonlinearity and time-variant properties of the weather has the advantage of quantitatively grasping the change in the demand of electricity based on the weather features from the perspective of the system operator. Finally, the described approach to determine the weights for combining modified load profiles can also be utilized. Future work will be focused on developing the proposed framework for more challenging work, such as reducing forecasting errors attributed to the inaccuracy of BTM PV generation forecasting.

REFERENCES

[1] S. S. Reddy, P. R. Bijwe, and A. R. Abhyankar, "Joint energy and spinning reserve market clearing incorporating wind power and load forecast uncertainties," *IEEE Syst. J.*, vol. 9, no. 1, pp. 152–164, Mar. 2015.

[2] S. S. Reddy, A. R. Abhyankar, and P. R. Bijwe, "Market clearing for a wind-thermal power system incorporating wind generation and load forecast uncertainties," in *Proc. IEEE Power Energy Soc. Gen. Meeting*, Jul. 2012, pp. 1–8.

[3] T. Hong, P. Pinson, Y. Wang, R. Weron, D. Yang, and H. Zareipour, "Energy forecasting: A review and outlook," *IEEE Open Access J. Power Energy*, vol. 7, pp. 376–388, 2020.

[4] G. Dudek, "Pattern-based local linear regression models for short-term load forecasting," *Electr. Power Syst. Res.*, vol. 130, pp. 139–147, Jan. 2016.

[5] A. Tarsitano and I. L. Amerise, "Short-term load forecasting using a two-stage sarimax model," *Energy*, vol. 133, pp. 108–114, Aug. 2017.

[6] P.-H. Kuo and C.-J. Huang, "A high precision artificial neural networks model for short-term energy load forecasting," *Energies*, vol. 11, no. 1, p. 213, Jan. 2018.

[7] S. S. Reddy and J. A. Momoh, "Short term electrical load forecasting using back propagation neural networks," in *Proc. North Amer. Power Symp. (NAPS)*, Sep. 2014, pp. 1–6.

[8] S. S. Reddy, "Bat algorithm-based back propagation approach for short-term load forecasting considering weather factors," *Electr. Eng.*, vol. 100, no. 3, pp. 1297–1303, Sep. 2018.

[9] I. Paliari, A. Karanikola, and S. Kotsiantis, "A comparison of the optimized LSTM, XGBOOST and ARIMA in time series forecasting," in *Proc. 12th Int. Conf. Inf., Intell., Syst. Appl. (IISA)*, Jul. 2021, pp. 1–7.

[10] J. Song, L. Jin, Y. Xie, and C. Wei, "Optimized XGBoost based sparrow search algorithm for short-term load forecasting," in *Proc. IEEE Int. Conf. Comput. Sci., Artif. Intell. Electron. Eng. (CSAIEE)*, Aug. 2021, pp. 213–217.

[11] F. Ziel, "Modeling public holidays in load forecasting: A German case study," *J. Mod. Power Syst. Clean Energy*, vol. 6, no. 2, pp. 191–207, Mar. 2018.

[12] S. Arora and J. W. Taylor, "Rule-based autoregressive moving average models for forecasting load on special days: A case study for France," *Eur. J. Oper. Res.*, vol. 266, no. 1, pp. 259–268, Apr. 2018.

[13] M. López, C. Sans, S. Valero, and C. Senabre, "Classification of special days in short-term load forecasting: The Spanish case study," *Energies*, vol. 12, no. 7, p. 1253, Apr. 2019.

[14] K. Zhu, J. Geng, and K. Wang, "A hybrid prediction model based on pattern sequence-based matching method and extreme gradient boosting for holiday load forecasting," *Electr. Power Syst. Res.*, vol. 190, Jan. 2021, Art. no. 106841.

[15] K.-B. Song, Y.-S. Baek, D. H. Hong, and G. Jang, "Short-term load forecasting for the holidays using fuzzy linear regression method," *IEEE Trans. Power Syst.*, vol. 20, no. 1, pp. 96–101, Feb. 2005.

[16] Y.-M. Wi, S.-K. Joo, and K.-B. Song, "Holiday load forecasting using fuzzy polynomial regression with weather feature selection and adjustment," *IEEE Trans. Power Syst.*, vol. 27, no. 2, pp. 596–603, May 2012.

[17] M. Sun, C. Feng, and J. Zhang, "Factoring behind-the-meter solar into load forecasting: Case studies under extreme weather," in *Proc. IEEE Power Energy Soc. Innov. Smart Grid Technol. Conf. (ISGT)*, Feb. 2020, pp. 1–5.

[18] E. Anastasio and J. Mulhern. (May 14, 2019). *Improving Load Forecast With Behind-the-Meter Solar Forecast*. Accessed: Mar. 20, 2021. PJM, Norristown, PA, USA. [Online]. Available: https://www.pjm.com/-/media/committees-groups/committees/oc/20190514/20190514-item-20-improving-load-forecast-with-btm-solar-forecast.ashx

[19] Korea Meteorological Administration. *KMA Local Weather Forecasts*. Accessed: Mar. 20, 2021. [Online]. Available: https://data.kma.go.kr/data/rmt/rmtList.do?code=420&pgmNo=572

[20] Korea Meteorological Administration. *KMA Automated Synoptic Observing System*. Accessed: Mar. 20, 2021. [Online]. Available: https://data.kma.go.kr/data/grnd/selectAsosRltmList.do?pgmNo=36

[21] Ministry of Environment. *Heating and Cooling Degree Days*. Accessed: Mar. 20, 2021. [Online]. Available: http://27.101.216.209/home/web/dictionary/read.do;jsessionid=zwJR+J3NAqsKllL5WfcG-wH6.mehome1?pagerOffset=280&maxPageItems=10&maxIndexPages=10&searchKey=&searchValue=&menuId=10448&orgCd=&boardMasterId=&dicSeq=282&decorator

[22] M. Espinoza, J. A. K. Suykens, R. Belmans, and B. D. Moor, "Electric load forecasting," *IEEE Control Syst. Mag.*, vol. 27, no. 5, pp. 43–57, Oct. 2007.

[23] R. Stull, "Wet-bulb temperature from relative humidity and air temperature," *J. Appl. Meteorol. Climatol.*, vol. 50, no. 11, pp. 2267–2269, 2011.

[24] M. G. Lawrence, "The relationship between relative humidity and the dewpoint temperature in moist air: A simple conversion and applications," *Bull. Amer. Meteorolog. Soc.*, vol. 86, no. 2, pp. 225–234, Feb. 2005.

[25] J.-S. Lee, K. R. Kim, C. Cho, M. Kang, J.-C. Ha, and D. S. Kim, "Evaluating the accuracies of the WBGT estimation models and their onsite applicability in Korea," *J. Korean Soc. Hazard Mitigation*, vol. 19, no. 4, pp. 53–63, Aug. 2019.

[26] Korea Meteorological Administration. (2009). *Discomfort Index*. Accessed: Mar. 20, 2021. [Online]. Available: https://www.kma.go.kr/HELP/basic/help_01_05.jsp

[27] L. P. Rothfusz, "The heat index 'equation' (or, more than you ever wanted to know about heat index)," National Oceanic and Atmospheric Administration, National Weather Service, Fort Worth, TX, USA, Office of Meteorology, Tech. Rep., 90-23, 1990.

[28] Korea Meteorological Administration. (2009). *Windchill*. Accessed: Mar. 20, 2021. [Online]. Available: https://www.weather.go.kr/weather/lifenindustry/li_asset/HELP/basic/help_01_07.jsp

[29] D. Maia-Silva, R. Kumar, and R. Nateghi, "The critical role of humidity in modeling summer electricity demand across the united states," *Nature Commun.*, vol. 11, no. 1, pp. 1–8, Dec. 2020.

[30] Seoul Tourism Organization. *The Republic of Korea's National Holidays*. Accessed: Mar. 20, 2021. [Online]. Available: https://english.visitseoul.net/national-holidays

[31] S. Yilmaz, J. Chambers, and M. K. Patel, "Comparison of clustering approaches for domestic electricity load profile characterisation—Implications for demand side management," *Energy*, vol. 180, no. 1, pp. 665–677, Aug. 2019.

[32] R. J. Hyndman and A. B. Koehler, "Another look at measures of forecast accuracy," *Int. J. Forecasting*, vol. 22, no. 4, pp. 679–688, Oct. 2006.

[33] M. A. Hall, "Correlation-based feature selection of discrete and numeric class machine learning," Dept. Comput. Sci., Univ. Waikato, Hamilton, New Zealand, Work. Paper 00/8, May 2000.

[34] K. S. Tang, K. F. Man, S. Kwong, and Q. He, "Genetic algorithms and their applications," *IEEE Signal Process. Mag.*, vol. 13, no. 6, pp. 22–37, Nov. 1996.
[35] W. D. Chang, "Nonlinear system identification and control using a real-coded genetic algorithm," *Appl. Math. Model.*, vol. 31, no. 3, pp. 541–550, 2007.
[36] M. Safe, J. Carballido, I. Ponzoni, and N. Brignole, "On stopping criteria for genetic algorithms," in *Proc. Brazilian Symp. Artif. Intell.* Berlin, Germany: Springer, 2004.
[37] K. Y. Lee and P. S. Mohamed, "A real-coded genetic algorithm involving a hybrid crossover method for power plant control system design," in *Proc. Congr. Evol. Comput. (CEC)*, 2002, pp. 1069–1074.

JIHOO SON received the B.S. degree from Korea University, Seoul, South Korea, in 2020, where she is currently pursuing the M.S. degree in electrical engineering. Her research interests include power system load forecasting and renewable energy forecasting.

JIWON CHA (Graduate Student Member, IEEE) received the B.S. degree in environmental health and electrical engineering from Korea University, Seoul, South Korea, in 2014, where he is currently pursuing the Ph.D. degree. His research interests include time-series forecasting, renewable generation, and electric vehicle.

HYUNSU KIM received the B.S., M.S., and Ph.D. degrees in atmospheric sciences from Pusan National University, Busan, South Korea, in 2016. From 2017 to 2018, he was a Postdoctoral Fellow with the Division of Environmental and Sustainability, The Hong Kong University of Science and Technology (HKUST), Hong Kong. He was also a Research Professor with Ewha Womans University, South Korea, in 2018. Since 2019, he has been a Senior Meteorologist with Korea Power Exchange, South Korea. His research interests include weather forecasting for electric power systems and power demand forecasting with renewable energy (photovoltaic and wind power generation).

YOUNG-MIN WI received the Ph.D. degree in electrical engineering from Korea University, Seoul, South Korea, in 2013. From 2013 to 2014, he worked with the Korea Electrotechnology Research Institute (KERI), South Korea. He is currently an Assistant Professor with the Department of Electrical and Electronic Engineering, Gwangju University, Gwangju, South Korea. His research interests include power system operation and planning, particularly in load forecasting and its applications.